Large deformation and amorphization of Ni nanowires under uniaxial strain: A molecular dynamics study

Paulo S. Branício* and José-Pedro Rino
Departamento de Física, Universidade Federal de São Carlos, Via Washington Luiz Km 235, 13565-905 São Carlos, São Paulo, Brazil
(Received 18 May 2000)

Molecular-dynamics simulations were employed to study deformations on nickel nanowires subjected to uniaxial strain at 300 K using a recently reported embedded-atom (many body) model potential. This embedded-atom model can reproduce exactly the experimental second-order and third-order elastic moduli as well as the phase stability, equation of state and phonon frequency spectra are also in good agreement with experiments. Strong influence was observed in the Young modulus and force constant due to surface effects when considering nanowires with different cross sections. Applying strain rates, from 0.05 to 15% ps^{-1}, we found elastic behavior up to 11.5% strain with corresponding stress of 9.4 GPa. At low strain rates ($<0.05\%$ ps^{-1}) the system passes through plastic deformations although keeping the crystalline structure. This ductile process is showed by several snapshots. At this low strain rate regime we observed that the nanowires shows superplasticity. For high strain rates ($\geqslant 7\%$ ps^{-1}) the system changes continuously from crystalline to amorphous phase. Although this amorphization occurs with no use of liquid quenching or introduction of chemical or physical disorder, so being a different and interesting process, the amorphous resulted is unstable. We studied this instability monitoring the recrystallization process.

I. INTRODUCTION

Almost two decades ago Parrinello and Rahman (PR) (Ref. 1) have extensively studied bulk Ni under uniaxial loads using the recently proposed molecular dynamics (MD) technique where the shape and size of the system can change according to the dynamics evolution. This formalism allows us to explore the behavior of systems under generalized external stress and was used by them on bulk Ni. PR have used the interaction potential described by Milstein and collaborators,[2–4] which is a generalized two-body Morse potential (we will henceforth call it simply Morse potential). Milstein *et al.* have used it in extensive calculations of stress-strain relations on Ni. PR extending this study explored the fcc-hcp structural transition that occurs above a critical compressive stress, and also verified the elastic limit applying tensile loading. The interest in the properties of Ni and other metal both theoretically as well as experimentally still remains. Recently Chantasiriwan and Milstein[5,6] using the embedded-atom method for a series of metals were able to obtain exactly the second-order and the third-order elastic moduli, excellent agreement in the pressure-volume curves, and reasonably good agreement among phonon dispersions.

It is known that metals crystallize at well defined structures: fcc for Ni, Al, Cu, Ag, Au, etc.; bcc for Fe, Nb, Mo, Rb, Li, etc. An amorphous metal phase can also be obtained using mainly two methods: (i) Making alloys with elements different in size and bonding (chemical disorder); (ii) Cooling a liquid fast enough in order to avoid crystallization. Ikeda *et al.*[7] have proposed a different way to form an amorphous metal. They showed that it is possible to transform continuously a perfect crystal of Ni or NiCu alloy, at constant temperature (300 K), into an amorphous system by application of sufficiently large strain rate. They found that it is necessary to apply a strain rate above 5% ps^{-1} in order to obtain a homogeneous disordered material similar to a liquid and with no evidence of plastic instability (necking) as expected in a ductile crystalline state. This high strain rate is only reached experimentally in high velocity impact and shock wave studies where temperature control as well as details of the dynamics structural changes become very difficult to analyze.

In the present work we report a deformation study on Ni nanowires under uniaxial strain using MD simulations. We investigated the effect of the nanowire cross section in the stress-strain relation, the plastic deformations that take place beyond the elastic limit, and the amorphization induced by high strain rates. We have used the isostress, isoenthalpic (NtH) ensemble, where N is the number of particles, t the stress and H the enthalpy, and the canonical. (NVT) ensemble, where V is the volume and T the temperature. The NVT simulation is necessary since it enable us to study the system beyond the elastic limit, as well as handle temperature appropriately. The paper is organized as follows. A brief discussion about the interatomic potential is presented in Sec. II. The preparation of the crystalline state, and simulations details, are presented in Sec. III. In Sec. IV we present the discussions of the MD results and comparison with other results. The main results are finally summarized at the conclusion in Sec. V.

II. INTERACTION POTENTIAL

The MD simulations were performed using the EAM model reported by Chantasiriwan *et al.*[5] in which the second- and third-order elastic moduli are exact, the phase stabilities, pressure-volume curves, and phonon spectra in good agreement with experiments. In this model the cohesive energy per atom is given by

$$E = F(\varrho) + \frac{1}{2}\sum \phi(r_i),$$

with

$$\varrho = \sum f(r_i),$$

where $\phi(r_i)$ is the electrostatic pair potential, $f(r_i)$ the spherically averaged electron-density function, $F(\varrho)$ the embedding energy and r_i is the distance between the reference atom and the surrounding atom *i*. The summation are over all atoms *i* in the crystal. The functional form for these functions reads

$$\phi(r_i) = A(r - r_m)^4 \times [1 + d_1 r + d_2 r^2 + d_3 r^3 + d_4 r^4 + d_5 r^5 + d_6 r^6],$$

$$f(r) = \frac{1 + b_1 \cos(\alpha r) + b_2 \sin(\alpha r)}{r^\beta},$$

$$F(\varrho) = E_{\mathrm{EOS}}(a^*) - \frac{1}{2} \sum \phi(r_i),$$

where for cubic crystals with lattice parameter *a*,

$$E_{EOS}(a^*) = -E_{coh}(1 + a^* + k a^{*3}) e^{-a^*} \quad \text{for } \frac{a}{a_0} \leqslant 0.95 \text{ or } \frac{a}{a_0} \geqslant 1.05,$$

$$E_{EOS}(a^*) = -E_{coh} + \omega_1 \left(\frac{a}{a_0} - 1\right)^2 + \omega_2 \left(\frac{a}{a_0} - 1\right)^3 + \sum_{i=1}^{4} \gamma_i \left(\frac{a}{a_0} - 1\right)^{i+3} \quad \text{for } 0.95 < \frac{a}{a_0} \leqslant 1.00,$$

$$E_{EOS}(a^*) = -E_{coh} + \omega_1 \left(\frac{a}{a_0} - 1\right)^2 + \omega_2 \left(\frac{a}{a_0} - 1\right)^3 + \sum_{i=1}^{4} \eta_i \left(\frac{a}{a_0} - 1\right)^{i+3} \quad \text{for } 1.00 < \frac{a}{a_0} \leqslant 1.05$$

with

$$a^* = (a - a_0)/\lambda a_0$$

and

$$\lambda = \sqrt{E_{coh}/9 V_0 B}.$$

Experimental values for unstressed reference state define the lattice parameter a_0, cohesive energy E_{coh}, volume per atom V_0, and the bulk modulus B which is chosen to fit the experimental $P-V$ relation. All other constants A, $d_i, b_1, b_2, \alpha, \beta$ are fitting parameters which are determined in order to reproduce unrelaxed vacancy formation energy, combination of elastic moduli, and values of atomic volume at zero pressure. r_m is a cutoff distance such that $\phi(r_i) = 0$ for $r \geqslant r_m$. Analytical values for this quantities as well the way it was obtained can be found in the original paper (Chantasiriwan *et al.*[5]). The EAM incorporate an approximation to the many-body interaction necessary to describe the physics of metallic bonding which is absent in the pair-potential scheme. An excellent review with applications can be found in Daw *et al.*[8]

III. MOLECULAR DYNAMICS PROCEDURE

Molecular dynamics simulations were performed to study fcc monocrystal Ni nanowires under uniaxial strain along the $\langle 001 \rangle$ crystallographic direction using the interaction described above. The Ni nanowires were prepared considering a finite number of unit cells (u.c.) in *x* and *y* directions, while the infinite wire was obtained applying periodic boundary conditions (pbc) in the *z* direction. The cross section of the nanowires are in the range of 300–5000 Å^2 (which means 5 to 20 fcc u.c. in *x* and *y* directions) and the length of the nanowire is initially 35.2 Å (10 fcc u.c. in *z* direction). Nanowires ten times bigger have also been simulated but the results observed were independent of the nanowire length. All the results were obtained at constant temperature using NVT ensemble based on the Nosé-Hoover chain dynamics to suitable control the temperature.[9–11]

Initially we calculate the stress-strain relation up to the elastic limit for nanowires with different cross section, but the same length. From these results we obtained the cross-section dependence in the elastic region. In each case the system was first heated to 300 K and thermalized over a period of 20 000 time steps ($\Delta t = 3.75 \times 10^{-15}$ s). After that we applied the tensile strain ε_{33} with increments of 0.5% in its total length. The system was then allowed to relax completely over $15\,000 \Delta t$ reaching thermodynamic equilibrium when the stress component σ_{33} was then calculated. Relaxation means that the tensile strain is kept constant during some amount of simulation time. The final configuration was used as input for the next strained configuration, and so on. The equilibrium configuration was monitored by looking the fluctuation (less than 1%) in the stress and total energy of the system.

To study in detail the plastic deformation process that arises beyond the elastic limit we use one nanowire with $5 \times 5 \times 10$ fcc u.c. following the scheme above. We let the system deform until the system fail.

We also applied constant strain rates from 0.05 to 15% ps^{-1} to study the deformations in the nanowires. In this case, the tensile strain ε_{33} was applied uniformly,[7] in increments of 0.5% after some time steps, in order to obtain the desired strain rate, for instance, to get a strain rate of 0.05% ps^{-1} a tensile strain is increased every 2670 time steps. The stress component σ_{33} was averaged after each strain increment has been applied. Structural information was obtained from pair distribution functions calculated at the final configurations as well from snapshots of the systems. Finally we study the recrystallization process that takes place when the high strain rate is discontinued. From the final amorphous configuration obtained applying the highest strain rate (15% ps^{-1}), the radial distribution functions was calculated over different periods of time, during the relaxation process, to check the current structure.

IV. RESULTS AND DISCUSSION

The stress-strain dependence with nanowires cross section up to the elastic limit is shown in Fig. 1. The nanowires have

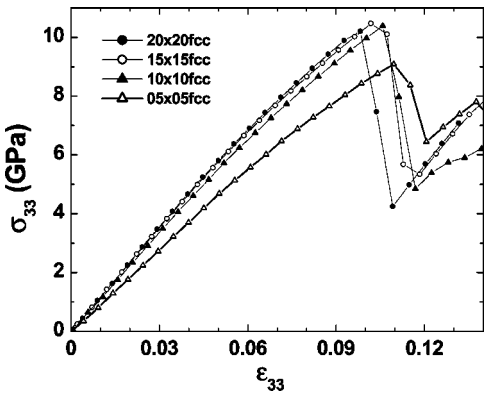

FIG. 1. Stress-strain curves for Ni nanowires with ten fcc unit cells long and different cross section at 300 K. For all nanowires the elastic limit is around 10.5% strain. The thicker nanowires presents considerable greater stress for any strain showing the explicit influence of the surface effects.

cross sections 5×5, 10×10, 15×15, and 20×20 fcc u.c. We can see that the elastic limit of the nanowires is reached at $\sim10.5\%$ strain (~9.5 GPa) and it is nearly independent of its cross section. However we can also note that, due to surface effects, the largest cross-section nanowire, 20×20 fcc u.c., presents stresses larger than that the 15×15 one, that is larger than that the 10×10 one, and so on. This fact shows the dependence of the stress-strain relation with the fraction of particles on the surface and in the volume of the nanowire, or, in other words, the energy per particle in the system. For all the results no hysteresis has been observed, and the initial configurations are recovered upon the removal of the load.

If we compare the yield stress obtained in this simulation (~9.5 GPa) with the value reported for a well annealed Ni of commercial purity we see that our result is more than 50 times bigger than that value (0.140 GPa). This overestimated result is, however, expected since in our simulation the nanowires are composed by pure and defect-free Ni. In contrast with real crystals where defects, like dislocations, which are the carriers of deformations, are always present. The experimental bulk sample have in general yield strengths far below the levels predicted by idealized calculations.[12] On the other hand, our results are only 2.5 times bigger than the yield stress reported for fine whiskers,[13] which are supposed to have no defects. However, the simulation results agree with recent studies on nanomaterials (nickel aluminide) which show that they are also much stronger than microstructured ones.[14]

Figure 2(a) displays the Young modulus of the nanowires obtained from Fig. 1 and Fig. 2(b) the force constant k, respectively. It can be seen that nanowires force constant scale linearly with cross-section area. Similar result has been observed for $SiSe_2$ nanowires.[15] Surface effects strongly affect both the Young modulus and the force constant.

Beyond the elastic limit the nanowires are not able to hold the structure and plastic deformations start to take place in order to accommodate the applied strain. Figure 3 displays the stress-strain curves for a Ni nanowire of cross section 5×5 fcc u.c. in which the applied strain rates vary from 0.05 to 15% ps^{-1} at 300 K. Roughly linear increase in stress occurs for all rates up to 11% strain. It is important to note that

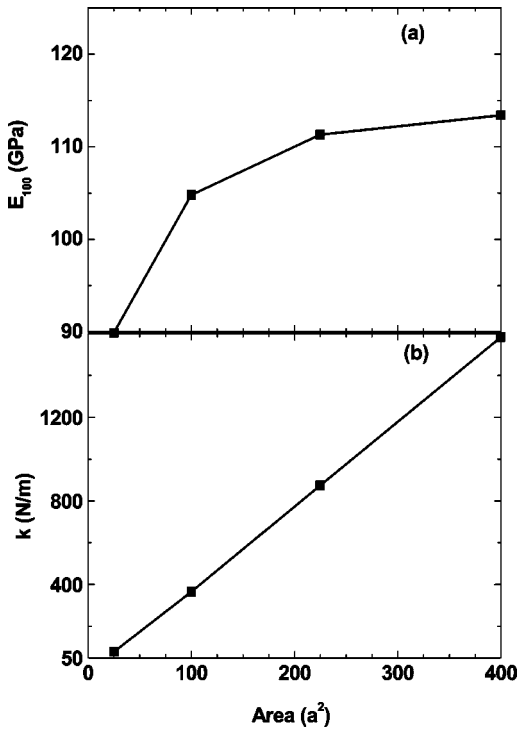

FIG. 2. Young modulus for the nanowires based on the results of Fig. 1 in (a) and corresponding force constant in (b). The area is in lattice parameter square units.

the stress and strain in the elastic limit observed is larger than the values reported by Ikeda *et al.* (5.5 Gpa and 7.5%) using Finnis Sinclair potential,[16,17] for nanowires with same cross section, 5×5 fcc u.c.

After the elastic limit has been overcame the stress falls substantially while a plastic deformation occurs (see Fig. 3). For strain rates smaller then 7% ps^{-1} the stress-strain curve shows a zigzag of increase-decrease in stress as the strain is increased. Cooperative displacement of the atoms in the nanowire, due to shear events (twinning), appears in the system in response to that. After each event the material keep

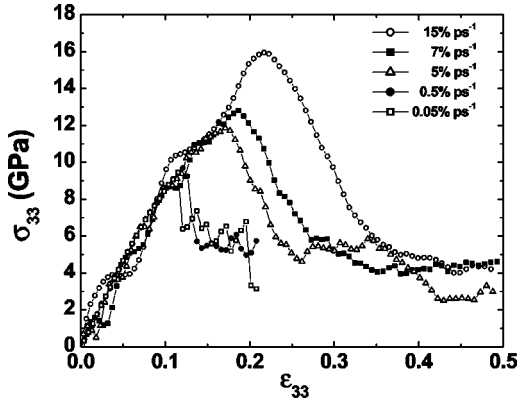

FIG. 3. Stress-strain curves for strain rates of 0.05 to 15% ps^{-1} starting from a single crystal at 300 K using the embedded-atom model (EAM). For all strain rates the system presents elastic behavior up to 11% strain. For 0.05 to 5% ps^{-1} the stress is relaxed by plastic deformation, which leads to a zigzag curve, more visible for small rates. For strain rates bigger or equal to 7% ps^{-1} there is a continuous transformation to the amorphous phase.

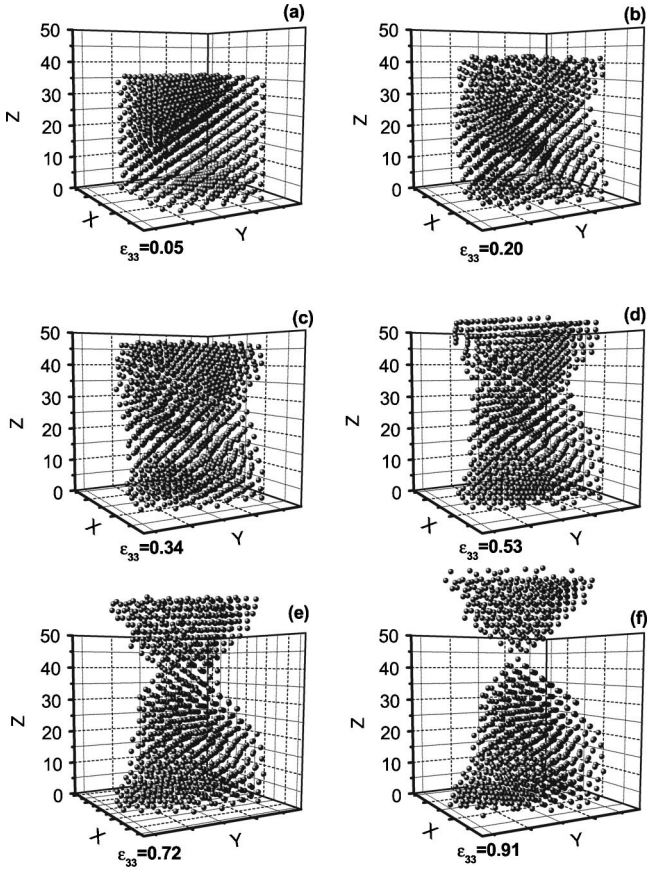

FIG. 4. Snapshots of a fcc Ni nanowire at several strain (0.05–0.91) starting from a single crystal at 300 K. At this strain rate (0.05% ps^{-1}) the system is almost completely relaxed. We can see in (a) the system before the elastic limit ($\varepsilon_{33}=0.11$) and in (b)–(f) the plastic deformations taking place beyond that. After 50% strain the necking formation occurs and culminate with failure of the nanowire at 91% strain.

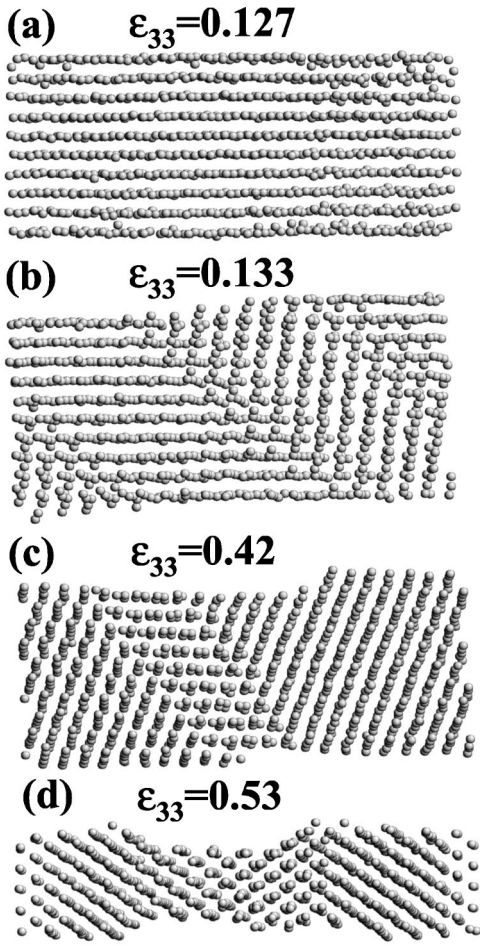

FIG. 5. Snapshots of a fcc Ni nanowire at several strain starting from a single crystal at 300 K under the strain rate 0.05% ps^{-1}. Different from Fig. 4, we can see the nanowire without perspective. In (a) and (b) we can see the structure right before and right after the first twinning. In (c) and (d) we can note the necking for further strain.

the new strucutre allowing the system to support higher stresses when the strain is increased. Figure 4 shows a series of snapshots of the system before and after the nanowire reach the elastic limit. These snapshots were obtained with the nanowire under 0.05% ps^{-1} strain rate. At this low strain rate the system is able to practically reach equilibrium condition between two successive application of strain. In Figs. 4(c) and 4(d) we can see lattice planes starting to slip. The stress relax during twinning formation due to large strain it causes for fcc crystals, see Hertzberg.[13] With strain larger than 50% we can note that the cyclical plastic deformation led to necking in the system, Figs. 4(e) and 4(f), which culminate with failure of the nanowire after strain bigger than 91%. In Fig. 5 we show a snapshot of the system at several stress loading were the twinning can be observed. We can also note in Fig. 4(f) that in our case the cross-section area of the neck goes to nearly zero when finally the system fails. The ratio between the final diameter and the initial diameter of the fractured portion of the nanowire can be evaluated. We observe that this ratio goes to zero at failure, and in addition the wire supports a large deformation (more than 90%). This behavior is often associated with superplasticity.[18]

Going back to Fig. 3 it can be seeing that from 0.05 to 5% ps^{-1} nearly the same behavior shown in Fig. 4 was found. Although the system is not in equilibrium, the nanowires remain crystalline during the cyclic deformation. The slower is the strain rate the closer of equilibrium the system will be and more crystalline it remains. For strain rates higher than 5% ps^{-1} we can observe a completely different behavior. The drops/raises cycle in the stress disappears, the stress-strain curve becomes smooth and the system changes homogeneously from the fcc crystal to a glasslike state. The maximum stress raise to near $\sigma_{33}=13$ (16) GPa for 7 (15)% ps^{-1} and softly fall to $\sigma_{33}=4$ GPa after 50% strain. Further straining the system we found a limit stress of $\sigma_{33}=2.9$ GPa for 100% strain. Figures 6 show some snapshots of the system deformed at 15% ps^{-1} rate at several strains from 7 to 48%. After 20% strain [Fig. 6(c)], when the stress starts to decrease (see Fig. 3), the system loses the crystalline structure and flow as an amorphous solid or a fluid and no necking is observed before its failure.

From the MD trajectories we can compute positional correlations such as the pair distribution function. Pair distribution function is calculated from $\langle n(r)\rangle \Delta r = 4\pi r^2 \rho g(r)$, where $n(r)\Delta r$ is the number of particles is a shell between $rer+\Delta r$ around a given particle. The angular bracket represent the ensemble average as well as an average over all

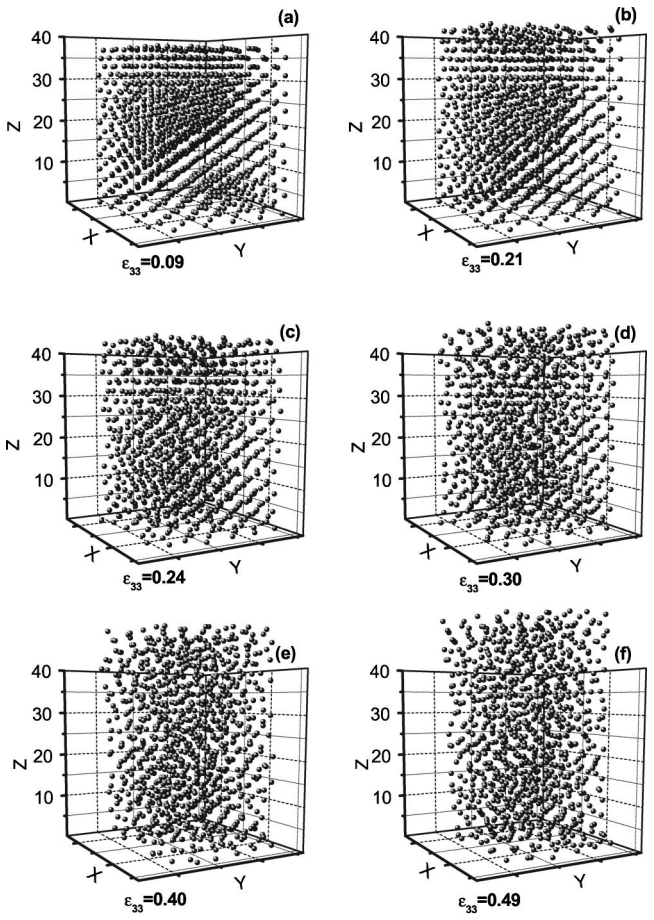

FIG. 6. Snapshots of a fcc Ni nanowire at several strains (0.09–0.49), deformed at uniform strain rate of 15% ps^{-1}, starting from a single crystal at 300 K using EAM. After the elastic limit is reached ($\varepsilon_{33}=0.22$) we can see the loss of crystalline lattice in (c)–(f), in a way completely different from Fig. 4. No necking formation is observed and the system flows as a liquid.

particles, and ρ is the number density. In Fig. 7 we display the radial distribution function for the final configuration, 50% strain, for all nanowires deformed at the strain rates shown in Fig. 3. These pair correlation functions were calculated considering only the last 100 time steps, which means that the system are not allowed to reach equilibrium,

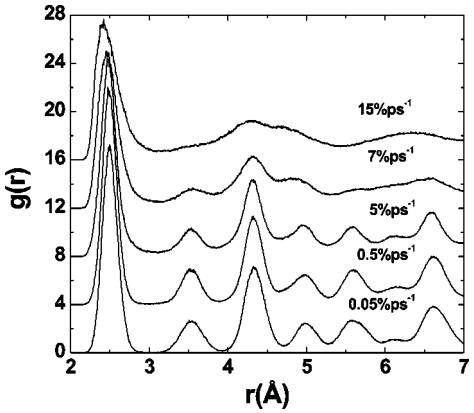

FIG. 7. Pair distribution function of Ni nanowires for strain rates from 0.05 to 15% ps^{-1} at 50% strain.

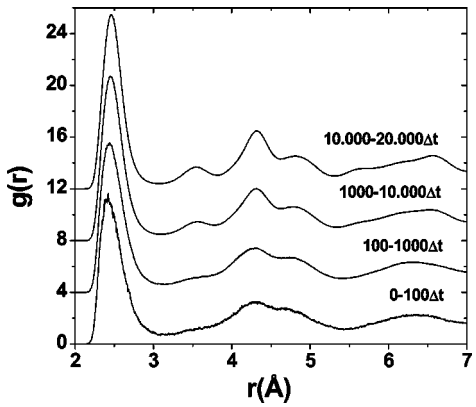

FIG. 8. Pair distribution functions of Ni nanowires starting at 50% strain, deformed at 15% ps^{-1} strain rate. While the functions were being calculated the strain was held constant. The recrystallization was monitored averaging $g(r)$ over different time intervals.

it shows the current structure at the final strained configuration. The crystalline structure is well defined up to 5% ps^{-1}. For strain rates bigger than 5% ps^{-1} the system starts to lose its long-range order and short-range order, that can be seen by the absence of correlations after 5 Å and the lowering of the second peak in $g(r)$, respectively. At 7% ps^{-1} the amorphous state is observed, very small oscillation after 5.0 Å and only a small bump around 3.5 Å in $g(r)$.

For 5% ps^{-1} the strain rate is not big enough to keep the amorphous phase and between increments in the strain the system begins to recrystallize, keeping the ordered fcc structure. The same behavior is found for the resulting amorphous obtained using 15% ps^{-1} when the strain is fixed or when the strain rate is lowered to 5% ps^{-1} or less. So the critical strain rate to obtain and keep the system amorphous is about 7% ps^{-1}. Ikeda *et al.*[7] using a different interaction potential found the same behavior for 5% ps^{-1}.

In order to explore the recrystallization process that takes place when the strain rate is discontinued, radial distribution functions were calculated for the final configuration obtained using 15% ps^{-1}. Figure 8 shows several curves calculated at different time intervals after the strain rate has been halted. It shows that up to $1000\Delta t$ the system remains amorphous, but after that, slowly goes through a recrystallization process that culminate in a crystalline strained phase. This crystalline phase observed is formed by various disoriented fcc crystal regions which are strained by the residual stress.

V. CONCLUSION

Molecular dynamics simulations were performed to study deformations on nickel nanowires subjected to uniaxial strain at 300 K based on a recent embedded atom model. We studied the dependence of the stress-strain curve with nanowire cross section up to the elastic limit. We found that surface effects allow the larger cross section nanowires to support greater stress for any given strain than smaller ones. The force constant was found to have a linear dependence with the cross section of the nanowires. Our results show that the elastic limit is reached at ~10.5% strain (~9.5 GPa) and it is nearly independent of its cross section. For strain rates lower than 7% ps^{-1} the system passes through plastic defor-

mations keeping the crystalline structure. Several snapshots of the system revealed this ductile character, including the necking of the nanowire before failure. The ratio of the initial unstressed cross section and the cross section just before the failure indicates that the nanowire is superplastic. For strain rates equal or higher than 7% ps^{-1} the system changes continuously from crystalline to amorphous phase. This result is slightly different of that observed by Ikeda *et al.*[7] who report the same behavior for strain rates equal or higher than 5% ps^{-1} using Finnis-Sinclair potential. This amorphization takes place with no use of liquid quenching or introduction of chemical or physical disorder, so being a different process, however, the amorphous result is unstable. We studied this instability monitoring the recrystallization process. From radial distribution functions we can see that to keep the amorphous state the system must be under strain rate equal to or higher than 7% ps^{-1}.

ACKNOWLEDGMENTS

This work was partially sponsored by the Conselho Nacional de Desenvolvimento Científico e Tecnológico (CNPq) and the Fundação à Pesquisa do Estado de São Paulo (FAPESP).

*Email address: ppsb@iris.ufscar.br

[1] M. Parrinello and A. Rahman, J. Appl. Phys. **52**, 7182 (1981).
[2] F. Milstein, J. Appl. Phys. **44**, 3825 (1973).
[3] F. Milstein, J. Appl. Phys. **44**, 3833 (1973).
[4] F. Milstein and B. Farber, Phys. Rev. Lett. **44**, 277 (1980).
[5] S. Chantasiriwan and F. Milstein, Phys. Rev. B **58**, 5996 (1998).
[6] F. Milstein and S. Chantasiriwan, Phys. Rev. B **58**, 6006 (1998).
[7] H. Ikeda, Y. Qi, T. Çagin, K. Samwer, W.L. Johnson, and W.A. Goddard III, Phys. Rev. Lett. **82**, 2900 (1999).
[8] M.S. Daw, S.M. Foiles, and M.I. Baskes, Mater. Sci. Rep. **9**, 251 (1993).
[9] G.J. Martyna, M.L. Klein, and M. Tuckerman, J. Chem. Phys. **97**, 2635 (1992).
[10] S. Nose, J. Chem. Phys. **81**, 511 (1984).
[11] W.G. Hoover, Phys. Rev. A **31**, 1695 (1985).
[12] M. F. Ashby and D. R. H. Jones, *Engineering Materials 1: An Introduction to their Properties & Applications*, (Butterworth-Heinemann, Cornwall, 1997), p. 93.
[13] R. W. Hertzberg, *Deformation and Fracture Mechanics of Engineering Materials*, (John Wiley & Sons, New York, 1976), pp. 44 and 116.
[14] R.S. Mishra, R.Z. Valiev, S.X. McFadden, and A.K. Mukherjee, Mater. Sci. Eng., A **252**, 174 (1998).
[15] W. Li, R.K. Kalia, and P. Vashishta, Europhys. Lett. **35**, 103 (1996).
[16] A.P. Sutton and J. Chen, Philos. Mag. Lett. **66**, 139 (1990).
[17] M.W. Finnis and J.E. Sinclair, Philos. Mag. A **50**, 45 (1984).
[18] T. Okabe, T. Hatayama, H. Takei, and M. Ikeda, in *Creep and Fracture of Engineering Materials and Structures*—Part I, edited by B. Wilshire and D. R. J. Owen (Pineridge Press, Swansea, 1984), p. 211.